In Situ Atomic-Scale Imaging of Phase Boundary Migration in $FePO_4$ Microparticles During Electrochemical Lithiation

Yujie Zhu, Jiang Wei Wang, Yang Liu, Xiaohua Liu, Akihiro Kushima, Yihang Liu, Yunhua Xu, Scott X. Mao, Ju Li, Chunsheng Wang,* and Jian Yu Huang**

Orthorhombic Li_xFePO_4 ($0 \le x \le 1$) system has attracted much attention for its application as a high power cathode material in lithium ion batteries.[1] Although the performance of this material has been greatly improved by cation doping, surface coating and size reduction,[2–4] the fundamental phase transformation mechanisms accompanying lithiation/delithiation are still controversial.[5–19] Theoretical calculations have revealed that the lithiation/delithiation in $LiFePO_4$ is highly anisotropic with lithium ion diffusion being mainly confined into the channels along the *b*-axis (space group *Pnma*).[20–22] Ex situ high resolution transmission electron microscopy (HRTEM) study of microsized $LiFePO_4$ demonstrated that the phase boundary (PB) between $LiFePO_4$ and $FePO_4$ tends to lie on the *bc* plane.[23] Several variants of the PB migration mechanism have been proposed, such as the "domino-cascade" model and the "new core-shell" model.[10,11] Singh et al. developed a comprehensive surface-reaction-limited intercalation theory and first predicted that the $LiFePO_4/FePO_4$ PB migrated perpendicular to the lithium ion insertion direction like a "travelling wave".[12] Recently, Tang et al. proposed an overpotential-dependent phase transformation model by considering both the anisotropic lithiation and misfit strain properties,[6,17] where crystal→amorphous transitions occur at intermediate overpotential, and crystal→crystal transitions occur at low as well as high overpotentials.[7] Under large overpotentials, the PB of $FePO_4/LiFePO_4$ was predicted to align on the *ac* plane instead of *bc* plane.[13] The solid solution mechanism was also proposed for nano-$LiFePO_4$,[14–16] which suggested a single-phase lithiation pathway rather than nucleation and growth of a second phase during lithiation/delithiation. Bai et al. quantitatively demonstrated that the expected phase transformation would be suppressed in nano-$LiFePO_4$ and the lithiation would follow a solid solution behavior if the discharge current exceeded a critical value.[15] However, the single-phase solid solution transition pathway usually is expected in nanosized particles (~40 nm diameter with sloping charge/discharge voltage curves),[16] and not in microsized particles.

Obviously, real-time atomic-scale observation of lithiation/delithiation of $LiFePO_4$ is critical to clarify the phase transformation mechanisms. However, such dynamic observations have not been achieved due to technical difficulties associated with the experiments. Here we report the first dynamic HRTEM observations of the PB migration in microsized $FePO_4$ single-crystals during electrochemical lithiation, providing the first direct atomic-scale evidence for the PB migration mechanism.

In situ HRTEM observation of electrochemical lithiation in $FePO_4$ was conducted in an all-solid electrochemical cell setup,[24,25] which consisted of a $FePO_4$ crystal working electrode, a naturally-grown Li_2O solid electrolyte, and a bulk lithium metal counter electrode (**Figure 1**a). The orthorhombic $FePO_4$ was obtained from chemical delithiation of $LiFePO_4$ which was synthesized from a hydrothermal method.[26] The crystal structures of both $LiFePO_4$ and $FePO_4$ were

Y. Zhu,[+] Y. Liu, Dr. Y. Xu, Prof. C. Wang
Department of Chemical and Biomolecular Engineering
University of Maryland
College Park, Maryland 20742, USA
E-mail: cswang@umd.edu
J. W. Wang,[+] Prof. S. X. Mao
Department of Mechanical Engineering and Materials Science
University of Pittsburgh
Pittsburgh, Pennsylvania 15261, USA
Dr. Y. Liu,[+] Dr. X. Liu, Dr. J. Y. Huang
Center for Integrated Nanotechnologies
Sandia National Laboratories
Albuquerque, New Mexico 87185, USA
Email: jyhuang8@yahoo.com
Dr. A. Kushima, Prof. J. Li
Department of Nuclear Science and Engineering
and Department of Materials Science and Engineering
Massachusetts Institute of Technology
Cambridge, Massachusetts 02139, USA
E-mail: liju@mit.edu
[+]These authors contributed equally to this work.

DOI: 10.1002/adma.201301374

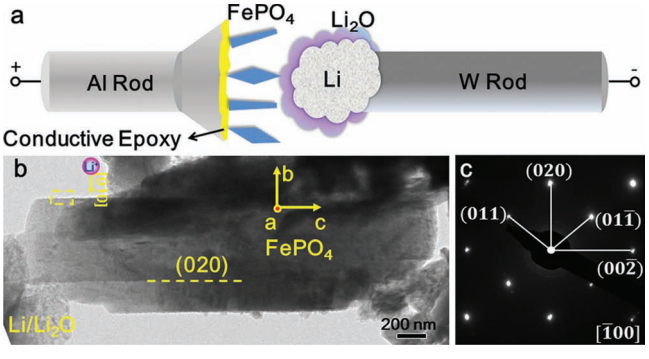

Figure 1. In situ TEM electrochemical experiment setup and morphology of $FePO_4$ crystal. (a) Schematic illustration of the in situ electrochemical cell. (b) A pristine $FePO_4$ crystal in [$\bar{1}$00] zone axis was connected with the Li_2O electrolyte to form an electrochemical device. The propagation of a phase boundary between $FePO_4$ and $LiFePO_4$ in the rectangle zone marked by yellow dashed line was captured in real time under HRTEM, as presented in Figure 2. (c) The electron diffraction pattern (EDP) of the $FePO_4$ crystal as shown in (b), indicating it is a single-crystal with the orthorhombic structure.

characterized by a powder X-ray diffraction (XRD) (Supporting Information Figure S1). The morphology of $FePO_4$ was characterized by a scanning electron microscopy (SEM) (Supporting Information Figure S2). The electrochemical behaviors of chemically delithiated $FePO_4$ were measured in a traditional liquid electrolyte cell (Supporting Information Figure S3), which showed well-defined voltage plateaus during both charge and discharge processes similar to the electrochemical behaviors of typical $LiFePO_4$ electrodes, demonstrating that the lithiation mechanism of chemically delithiated $FePO_4$ also reflects the lithiation mechanism of electrochemically delithiated $FePO_4$.[27] More experimental details (materials synthesis, in situ experiment set up and data processing procedure) are provided in Experimental Section and Supporting Information.

Figure 1b presents a TEM image of a pristine $FePO_4$ crystal connected to the Li_2O electrolyte. The electron diffraction patterns (EDPs) of the $FePO_4$ crystal (Figure 1c and Supporting Information Figure S4) indicated that it was a single-crystal with the orthorhombic structure, and the growth direction was [001] (Supporting Information Figure S4). Before lithiation, the $FePO_4$ crystal was tilted into [$\bar{1}$00] zone axis (Figure 1c) and the maximum thickness of the particle along this axis was around 300 nm (Supporting Information Figure S5). Different from many anode materials (Si, Sn etc.), the volume change for $FePO_4$ upon lithiation is only 7%, which is too small to be observed at a low magnification TEM image. So HRTEM was used to follow the lithiation process.

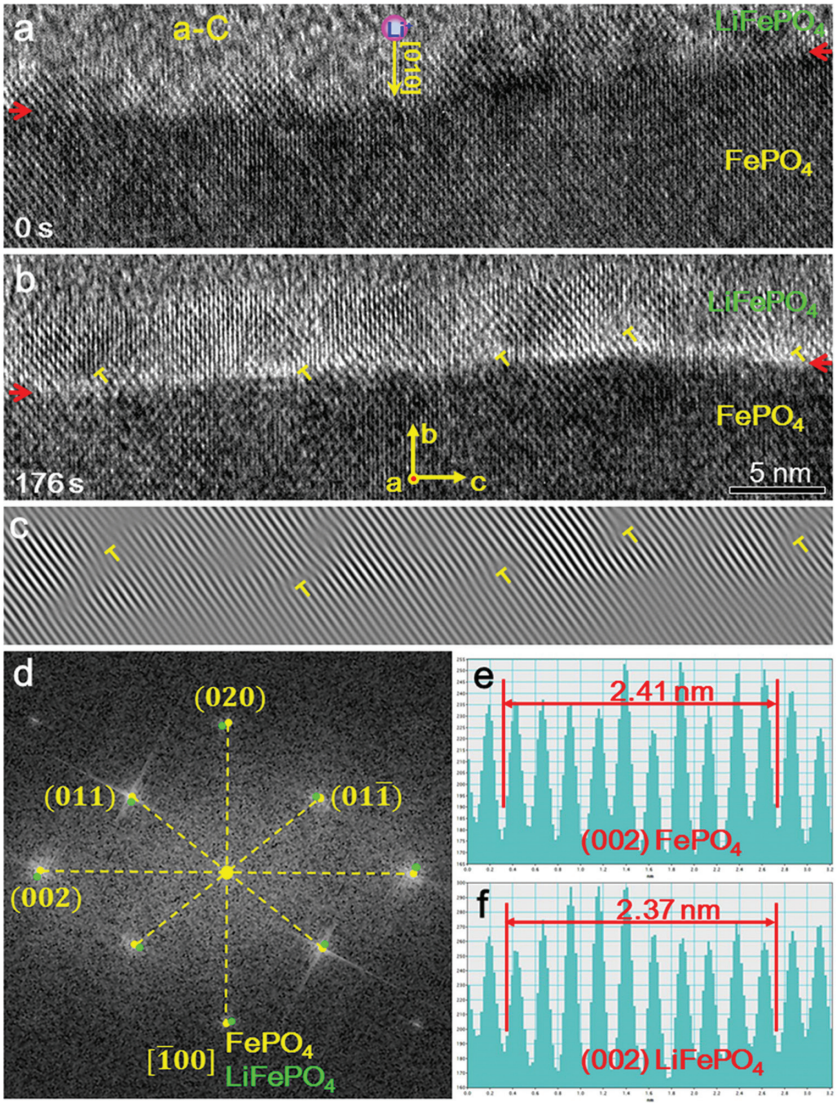

Figure 2. Migration of phase boundary between $FePO_4$ and $LiFePO_4$ along the [010] direction during lithiation. (a) After re-turning on the electron beam, a clear phase boundary between $FePO_4$ and $LiFePO_4$ was already developed due to lithiation, as pointed out by the red arrows. A layer of 10 nm amorphous carbon (a-C) was deposited on the surface of $FePO_4$ crystal to decrease the electron beam induced damage. (b) At 176 s, the thickness of the $LiFePO_4$ layer increased. The phase boundary was pointed out by the red arrows. The invert "T" marks mismatch dislocations at the phase boundary. (c) Inverse FFT (IFFT) image of (b), showing the distribution of mismatch dislocations near the phase boundary. (d) The FFT patterns of $FePO_4$ and $LiFePO_4$ produced from $FePO_4$ and $LiFePO_4$ regions in (b). To make comparison, FFT pattern of $LiFePO_4$ (green) was overlaid with that of $FePO_4$ (yellow). (e,f) Lattice spacing of (002) plane from $FePO_4$ and $LiFePO_4$ was measured from HRTEM image shown in (b), showing the lattice spacing of (002) plane decreased about 1.7% after lithium ion insertion into $FePO_4$.

Figure 2 shows HRTEM images of the PB evolution, from the rectangular zone in Figure 1b, during lithiation of $FePO_4$. The thickness along *a*-axis for this HRTEM observation region is less than 300 nm (Supporting Information Figure S5). A positive voltage of 2 V versus lithium metal was applied to the $FePO_4$ crystal in Figure 2 to drive lithium ion insertion into the crystal. To increase the conductivity and decrease the electron beam damage to $FePO_4$, 10 nm amorphous carbon (a-C) was coated on the surface of $FePO_4$ crystals (Figure 2a) and weak electron beam was used for imaging. To further minimize the electron beam damage to the sample, the electron beam was blanked immediately after the voltage was applied, and was re-turned on 10 min later to take the HRTEM images. It was found that below the a-C coating layer, a thin layer of $LiFePO_4$ was already formed on the surface of $FePO_4$ due to lithium insertion (Figure 2a). A clear PB (pointed out by the red arrows in Figure 2a), as evidenced by the image contrast and the misfit strain near the PB, was developed between $FePO_4$ and $LiFePO_4$ due to lithium ion insertion. After 176 s, a thicker $LiFePO_4$ layer (pointed out by red arrows in Figure 2b) was developed. The PB migrated from the surface inward the core as more lithium ions were inserted into the $FePO_4$ (Supporting Information Figure S6). From the displacement of PB (Supporting Information Figure S7), the corresponding discharge C-rate for the particle is roughly estimated to be 0.1C. The PB was clearly a sharp interface (Figure 2a, b), which is

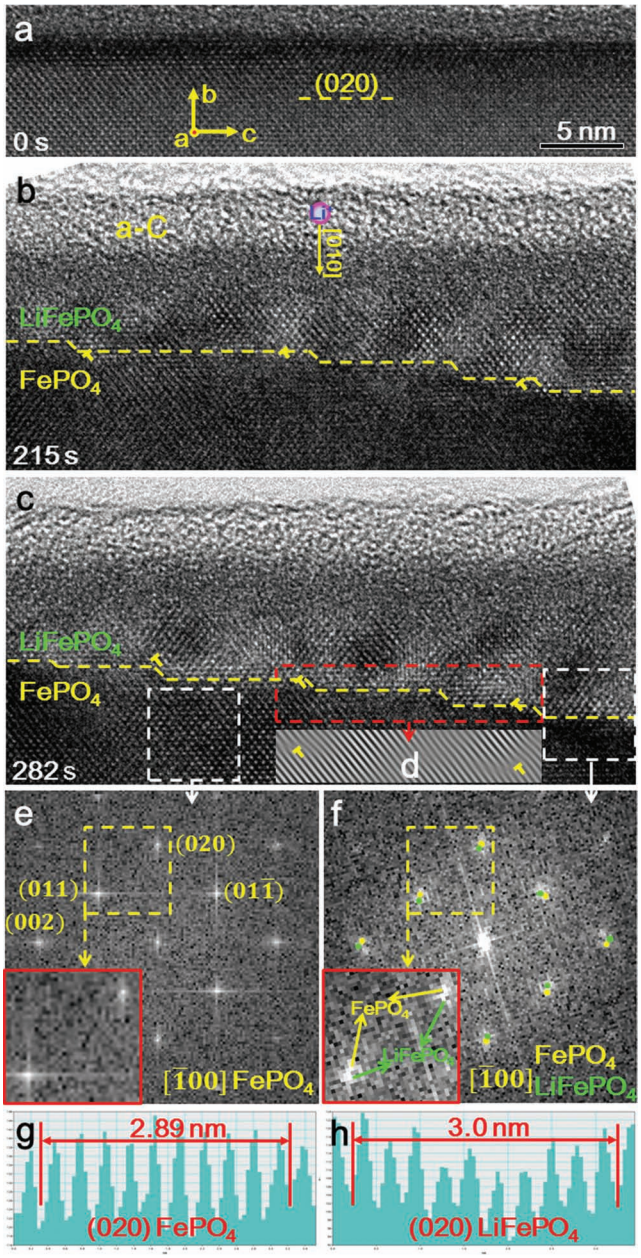

Figure 3. Step-like phase boundary between $FePO_4$ and $LiFePO_4$ and its migration along the [010] direction during lithiation. (a) A HRTEM image of the pristine $FePO_4$ in [$\bar{1}$00] zone axis. The crystal orientation and (020) plane were denoted. (b) At 215 s after applying the voltage, a step-like phase boundary was formed between $FePO_4$ and $LiFePO_4$, as pointed out by the yellow dashed line. (c) At 282 s, the thickness of the $LiFePO_4$ layer increased as the step-like phase boundary propagating along the [010] direction. The regions, marked by white dashed lines, show where we took the FFT patterns for $LiFePO_4$ and $FePO_4$ phases. The inset image shows Figure 3d. (d) Inset of (c) with inverse FFT (IFFT) image from the rectangle zone marked by red dashed line in (c), showing the lattice mismatch induced dislocations at the phase boundary between $FePO_4$ and $LiFePO_4$.(e) The FFT pattern of $FePO_4$ side showing sharp single spots at each diffraction points. The inset image shows that each diffraction spots do have one point. (f) The FFT pattern of the $LiFePO_4$/$FePO_4$ co-existing zone. Two sets of diffraction patterns are identified to be $LiFePO_4$ and $FePO_4$, respectively. The inset image shows that each diffraction spots do split into two points. (g,h) Lattice spacing of (020) plane for $FePO_4$ and $LiFePO_4$.

consistent with the electron energy loss spectroscopy (EELS) study reported by Laffont et al.[11] in which the PB was shown to be the juxtaposition of $FePO_4$ and $LiFePO_4$ rather than a solid solution region with a concentration gradient. EELS characterization was performed on both the pristine $FePO_4$ and the $LiFePO_4$ generated by in situ lithiation for the particle in Figure 2, and the results confirmed formation of $LiFePO_4$ in $FePO_4$ (Supporting Information Figure S8 and corresponding text).[11] Detailed analyses of the HRTEM images (see data processing procedure for HRTEM images in Supporting Information) indicated that the PB was nearly parallel to the *ac* plane, and it migrated along the *b*-axis inward. It is worth noting that although the $FePO_4$ crystal was connected with Li_2O solid electrolyte on the left edge where *ab* face was exposed (Figure 1b), the lithium ion insertion did not occur along the *c*-axis but along the *b*-axis which is far away from the lithium source, indicating that lithium ion was inserted into $FePO_4$ only along the *b*-axis of $FePO_4$ crystal, probably after transported via surface diffusion. The one-dimensional lithiation mechanism along the [010] direction (*b*-axis) is in accordance with theoretical calculations.[20–22] Therefore, our in situ HRTEM observation provides the first direct evidence for the anisotropic lithiation mechanism in $FePO_4$.

The phase transformation from $FePO_4$ to $LiFePO_4$ induces nearly periodic array of dislocations on the $FePO_4$ side at the PB, as outlined by the inverted "T" in Figure 2b,c. Figure 2d presents the superimposed Fast Fourier Transformation (FFT) patterns of $FePO_4$ (yellow dots) and $LiFePO_4$ (green dots) produced from the HRTEM image (Figure 2b). Obviously, after lithiation, the orientation of newly formed $LiFePO_4$ slightly rotated comparing with $FePO_4$, which was also observed by Chen et al.[23] in chemically delithiated $Li_{0.5}FePO_4$ using *ex situ* HRTEM. This may be attributed to inhomogeneous elastic deformation of the particle to accommodate the transformation strain. Also, as shown in Figure 2e-f, after $FePO_4$ was transformed into $LiFePO_4$, the lattice spacing of the (002) plane decreased about 1.7%, which is close to the theoretically expected lattice difference between $FePO_4$ and $LiFePO_4$ in this direction, i.e. 1.9%. If the PB was fully coherent, the lattice constant near PB should be quite different from the stress-free lattice constant of the particular phase, and should approach the mean of the two phases. The fact that the measured lattice constants are quite close to the stress-free lattice constants means majority of the elastic misfit energy along this direction has indeed been relaxed away, due to the presence of the misfit dislocations.

The PB migration mechanism is repeatable in our experiments. **Figure 3** are the HRTEM images showing the PB migration in another $FePO_4$ single-crystal during lithiation. A positive voltage of 2.7 V versus lithium metal was applied to the $FePO_4$ crystal. The pristine $FePO_4$ crystal had a uniform thickness (Supporting Information Figure S9) and was coated with a thin layer of a-C (Figure 3a). After lithiation for 215 s, a PB on the (020) plane with few steps was formed between $FePO_4$ and $LiFePO_4$, as marked by the yellow dashed line in Figure 3b, and the lithium ion insertion direction was also [010] direction (*b*-axis). The step-like PB might be caused by the lithium ion concentration gradient along the a-C thin layer, where the right portion of the particle had higher lithium ion concentration because it was closer to the lithium source (Supporting

Information Figure S9). After another 67 s, the thickness of the $LiFePO_4$ layer increased as the step-like PB propagating along the [010] direction (Figure 3c), and it was found that these steps moved along the [010] direction by simply following the movement of PB. Figure 3d (inset of Figure 3c) presents the inverse FFT (IFFT) image from the rectangle area, marked by red dashed line in Figure 3c, showing the mismatch dislocations at the PB, which is similar to the results shown in Figure 2c. The FFT patterns, from both the single-phase $FePO_4$ and the two-phase $FePO_4$/$LiFePO_4$ regions marked by white dashed squares in Figure 3c, were shown in Figure 3e,f, respectively. For the $FePO_4$ region, very sharp single diffraction spots were observed in the pattern (Figure 3e and its inset). However, the diffraction spots in the FFT pattern from the two-phase $LiFePO_4$/$FePO_4$ region were split, showing two sets of FFT patterns (Figure 3f and its inset) and diffuse intensity distributions, which is obviously different from the single-phase pattern shown in Figure 3e. By measuring the lattice spacing in Figure 3f, one set of the FFT pattern was identified as $LiFePO_4$, while the other was from $FePO_4$. As shown in Figure 3g,h, after $FePO_4$ was transformed into $LiFePO_4$, the lattice spacing of the (020) plane increased by about 3.8%, which is consistent with the theoretical lattice misfit value (i.e. 3.6%) in this plane. Besides the two particles presented in Figures 2 and 3, the third $FePO_4$ particle was also studied and showed the similar results (Supporting Information Figure S10). These similar results further confirmed that the dynamic PB in the $FePO_4$ microparticles was parallel to the (010) plane, and its propagation direction was along [010].

The theoretical misfit strains along *a*, *b* and *c* directions between $LiFePO_4$ and $FePO_4$ are $\delta_{[100]} = 5\%$, $\delta_{[010]} = 3.6\%$, and $\delta_{[001]} = -1.9\%$,[28] respectively. It is obvious that *a*-axis misfit contributes the most to the elastic misfit strain, which unfortunately we were not able to observe due to the zone axis condition in imaging. However, the dislocation nucleation is so favorable, as shown in Figures 2 and 3, that at room temperature even a small misfit strain of 1.9% can drive it. This implies that the larger misfit strain of 5.0% in *a*-axis, which ought to give larger driving force for dislocation nucleation, should sustain significant coherency loss efficiently as well. In Figure 2b, we count 5 misfit dislocations over a length of ~45 nm along the *c*-axis. The Burgers vector was identified to be [011]/2 (Supporting Information Figure S10 d). So the contribution to *c*-axis misfit displacement per dislocation was 4.7 Å/2 = 2.35 Å, and five dislocations would contribute 2.35Å ×5 = 11.75 Å of inelastic accommodation in *c*-axis with 11.75 Å/ 45 nm = 2.6%, which is very close to the theoretical mismatch of 1.9% in *c*-axis, given the statistical sampling errors in a small view field. Thus, the system is able to generate just the right density of dislocations to nearly entirely cancel out the misfit elasticity strain in *c*-axis. Dislocation nucleation was apparently facile in this system, which enables the coherency loss. Dislocation migration was also sustainable, since the dislocations appeared to follow the motion of the chemical interface (Supporting Information Figure S6).

Previous theoretical models assumed that the differences in lattice constant between $LiFePO_4$ and $FePO_4$ are entirely taken up as elastic strain energy when phase transformation happens,[6,10] giving rise to local stress as high as ~1 GPa. Such a high stress may couple into lithium migration and give rise to interesting physical effects such as exceedingly fast PB migration in nanosized $LiFePO_4$.[10] However, our in situ experiment reveals that, at least for particles with facile generation of misfit dislocations, the elastic strain energy term should be greatly reduced. Facile generation of misfit dislocations should favor the particle to be a two-phase mixture with a sharp interface between $Li_{1-x}FePO_4$ and Li_xFePO_4 ($x \sim 0$) phases, rather than as a single-phase solid solution (no solubility gap), since the elastic coherency energy closes up the spinodal gap and delays or prevents the onset of concentration wave instability of supersaturated homogenous solid solution.[15] While the coherency loss caused by misfit dislocations favors the $LiFePO_4$/$FePO_4$ two-phase transition mechanism, it also has a significant effect on the PB orientation. As recently suggested by Cogswell et al.[29] through a fully anisotropic analysis, a fully coherent PB between $LiFePO_4$ and $FePO_4$ would align on the (101) plane which was shown to be the lowest energy orientation. The observed (100) PB by *ex situ* HRTEM was attributed to a partial loss of coherency along *c*-axis.[23] In our study, the observed (010) PB is a consequence of even more severe coherency loss, since we clearly observed coherency loss happened along both *b*- and *c*-axis, and it was also highly favorable along *a*-axis as discussed above. Different strain relaxation mechanism along *a*-axis might alter the picture of observed phase boundary orientation because the lattice misfit is the largest along this axis. Also, in reference to Tang et al.'s lithiation model,[13,17] while a high overpotential may override the thermodynamic consideration of strain energy and rotates the (100) inclined PB towards kinetics-controlled (010) inclination, introducing the misfit dislocations would serve a similar purpose, by reducing the strain energy itself.

While the introduction of misfit dislocations has significant impacts on the thermodynamics of Li_xFePO_4 ($0 < x < 1$) system, it also influences the kinetic processes of phase transformation. First, the coherent PB to semicoherent PB transition is itself a thermally activated, size-dependent process with possibility of hysteresis, and depends sensitively on "extrinsic" or processing-dependent factors such as crystalline quality of the particle, confinement of nearby particles and binder, etc., which are not necessarily just functions of the particle size. Second, while the presence of misfit dislocations reduces the total energy of system, they also "pin" the chemical interface, in the sense that they need to co-move with the advancing chemical front by climbing, which is another thermally activated dissipative process that is generally quite slower than a coherent displacive process.[10]

Figure 4 shows the dynamic lithiation mechanism discovered in this study. With lithium ion insertion only along the [010] direction, the reduction of lattice misfit strain energy by dislocations favors the two-phase transition mechanism and changes the PB from the thermodynamics-controlled (100) plane (or (101) plane) to kinetics-controlled (010) plane.[29] Our in situ HRTEM observations provide evidence that microscopic damage in the form of nucleated dislocations accompanies chemical transformations in microparticles. These dislocations are expected to accumulate during electrode cycling, which could form preferential sites for cracking. This is expected to be a general degradation mechanism in Li intercalation

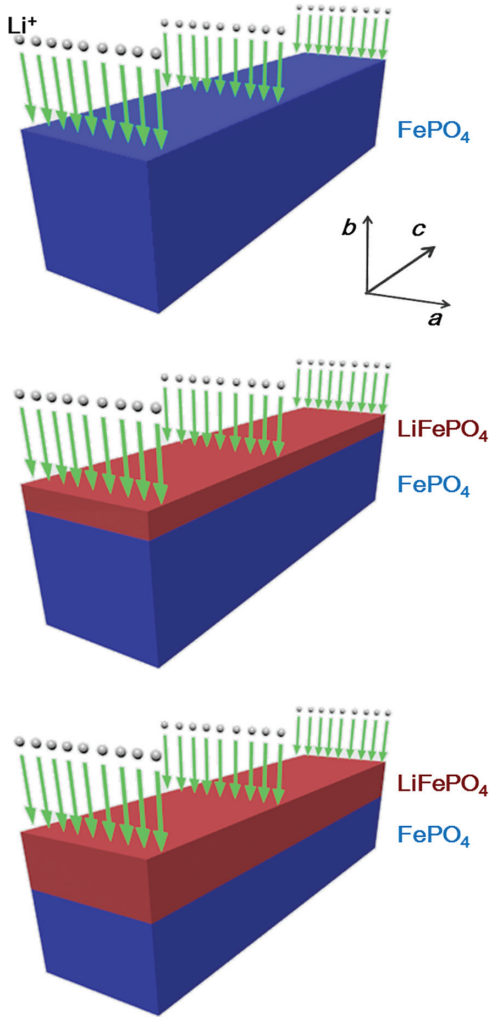

Figure 4. Schematic illustrations of lithiation mechanism discovered in this study. The migration direction of the phase boundary is the same as the lithium ion diffusion direction (i.e. [010] direction), which was observed in this study (Figures 2 and 3). The green arrows mark the lithium ion insertion direction.

compounds. Here, it needs to be emphasized that the $FePO_4$ particles studied here are microsized, so the lithiation mechanism is expected to change when the sample goes down to nanoscale as suggested by recent studies.[28–31] It has been shown that particle size, as well as electrode nanostructures (such as porous electrode etc.), plays a critical role on determining the phase behavior of Li_xFePO_4 system.[14–16,27–32] For example, Weichert et al.[27] recently studied the PB propagation in a $LiFePO_4$ particle, whose size was much larger than the samples in present study, upon chemical delithiation by in situ optical microscopy and the PB was shown to migrate along the [001] direction (*c*-axis). which was clearly different from the present and previous HRTEM results.[23] Also, significant amount of cracks were observed and the formed $FePO_4$ was highly porous. The transformation was shown to be diffusion-limited due to the large length scale. Decreasing the sample size to nanoscale would result in a different regime. Besides the short ion transport length, it has been shown that the lithium ion diffusivity in nanoparticles is much higher than that in the bulk materials.[30] Also, it would be more difficult for dislocations to nucleate in smaller particles,[33] and a coherent PB is preferable in nanoparticles. This is supported by previous study in which the 43-nm $LiFePO_4$ particle was shown to have a much higher retained strain than the 113-nm sample when two samples were at the same state-of-charge.[28] The coherency strain also changed the phase diagram in Li_xFePO_4 system,[29] specifically, stabilizing the solid solution at relatively low temperature and shrinking the miscibility gap between $FePO_4$ and $LiFePO_4$.

Cycle life and capacity fading of batteries are closely related to the fatigue of electrodes, which is caused by accumulation of microscopic damage defects such as dislocations during electrochemical cycling, that eventually leads to cracking.[23,27] We have identified a detailed pathway where dislocations may be generated, due to coherency loss transition during electrochemical lithiation. Since coherency loss is more likely in microsized particles than in nanosized particles, from well-known size effect similar to that of epitaxial thin film growth and alloy precipitation, we can predict that nanosized particles should have better fatigue life. Also, the accumulation of dislocations may lead to amorphization, which was observed in many electrode materials during electrochemical cycling.[7] Recently, solid-state amorphization due to accumulation of dislocations has been directly observed.[34,35]

In summary, we report the first real-time atomic-scale observation of the phase boundary migration mechanism and the anisotropic lithiation in $FePO_4$ microparticles. The phase boundary was shown to align along the (010) plane and move towards the [010] direction which is the same as the lithium ion diffusion direction. This result was shown to be caused by relaxation of majority of the elastic strain energy, as demonstrated by the observed periodic dislocations along the phase boundary and the measured lattice spacings which are quite close to the stress-free lattice constants of $FePO_4$ and $LiFePO_4$. Our in situ observation provided clear evidence for the phase boundary migration mechanism in microsized $FePO_4$/$LiFePO_4$ system. The results reported here constitute the first real-time atomic-scale experimental evidence of the phase transformation mechanism in $FePO_4$/$LiFePO_4$ system, which is currently under intensive experimental and theoretical investigations.

Experimental Section

Materials synthesis and characterization: $LiFePO_4$ was synthesized using a hydrothermal method.[26] LiOH aqueous solution (10 mL of 4 M) was mixed with aqueous solution (5 mL) of H_3PO_4 (0.015 mol) and $(NH_4)_2HPO_4$ (0.005 mol) to form a white suspension. Then, $FeSO_4{\cdot}7H_2O$ aqueous solution (10 mL of 2 M) was slowly added into above suspension with continuous stirring and argon purging. The molar ratio of Li:Fe:P was kept at 2:1:1. The mixture was transferred to a Parr autoclave, which was then held at 180 °C for 12 h. After natural cooling to room temperature, the product was collected and washed with ethanol and deionized (DI) water for several times. The final product was dried at 80 °C in a vacuum oven for overnight.

$FePO_4$ was obtained from chemical delithiation of $LiFePO_4$ using nitronium tetrafluoro-borate NO_2BF_4 in acetonitrile. $LiFePO_4$ (0.1 g) was added into a solution of NO_2BF_4 (0.17 g) in acetonitrile (10 mL). The mixture was stirred for 24 h at room temperature with continuous Ar bubbling, followed by centrifugation and washing with acetonitrile and

DI water for several times. The product was dried at 80 °C in a vacuum oven for overnight. The crystal structures of both $LiFePO_4$ and $FePO_4$ were characterized by a powder X-ray diffraction (XRD) (Supporting Information Figure S1). Both XRD patterns were indexed in the orthorhombic (*Pnma*) crystallographic system (Supporting Information Figure S1) and showed that there were no detectable impurities in the samples. The morphology of obtained $FePO_4$ was characterized by SEM. The results are shown in Figure S2. The electrochemical responses of $FePO_4$ were tested and shown in Figure S3. The orientation of $FePO_4$ crystals was determined by HRTEM and the results were shown in Figure S4. Figure S5 shows a double tilt experiment for a typical $FePO_4$ particle.

Set up of the in situ HRTEM experiment: For the in situ HRTEM experiment, the $FePO_4$ crystals were glued onto the aluminum rod with conductive epoxy. Fresh lithium metal was scratched from a fresh cut lithium metal surface by using a tungsten wire inside a glove box, and transferred into the TEM using a sealed bag filled with dry helium. During the transfer process, the lithium metal was exposed in air for about 2 s. The naturally-grown Li_2O served as the solid electrolyte. It has been shown that Li_2O can be functioned as an effective solid electrolyte for the lithium ion transport.[24,25] The Li/Li_2O was driven to contact the $FePO_4$ crystal using a piezomanipulator (Nanofactory transmission electron microscopy–scanning tunneling microscopy (TEM-STM) holder). Comparing with the conventional liquid cell, this kind of solid cell offers the advantage of direct observation of the microstructure evolution inside TEM, especially for the in situ HRTEM.

Supporting Information

Supporting Information is available from the Wiley Online Library or from the author.

Acknowledgements

This work is supported as part of the Nanostructures for Electrical Energy Storage, an Energy Frontier Research Center funded by the U.S. Department of Energy, Office of Science, and Office of Basic Energy Sciences under Award Number DESC0001160. Financial support in part by the National Science Foundation under Contract No. CBET0933228 (Dr. Maria Burka, Program Director) is gratefully acknowledged. A. K. and J. L. acknowledge support by NSF DMR-1008104 and DMR-1120901. The authors acknowledge the technical support of the NanoCenter in University of Maryland. Portions of this work were supported by a Laboratory Directed Research and Development (LDRD) project at Sandia National Laboratories (SNL). The LDRD supported the development and fabrication of platforms. The NEES center supported the development of TEM techniques. CINT supported the TEM capability. Sandia National Laboratories is a multi-program laboratory managed and operated by Sandia Corporation, a wholly owned subsidiary of Lockheed Martin Corporation, for the U.S. Department of Energy's National Nuclear Security Administration under contract DE-AC04-94AL85000.

Received: March 26, 2013
Revised: June 6, 2013
Published online: July 21, 2013

[1] A. K Padhi, K. S. Nanjundaswamy, J. B. Goodenough, *J. Electrochem. Soc.* **1997**, *144*, 1188.
[2] S. Y. Chung, J. T. Bloking, Y. M. Chiang, *Nature Mater.* **2002**, *1*, 123
[3] B. Kang, G. Ceder, *Nature* **2009**, *458*, 190.
[4] X. L. Wu, L. Y. Jiang, F. F. Cao, Y. G. Guo, L. J. Wan, *Adv. Mater.* **2009**, *21*, 2710.
[5] C. V. Ramana, A. Mauger, F. Gendron, C. M. Julien, K. Zaghib, *J. Power Sources* **2009**, *187*, 555.
[6] M Tang, J. F. Belak, M. R. Dorr, *J. Phys. Chem. C* **2011**, *115*, 4922.
[7] Y.-H. Kao, M. Tang, N. Meethong, J. Bai, W. C. Carter, Y.-M. Chiang, *Chem. Mat.* **2010**, *22*, 5845.
[8] V. Srinivasan, J. Newman, *J. Electrochem. Soc.* **2004**, *151*, A1517.
[9] A. S. Andersson, J. O. Thomas, *J. Power Sources* **2001**, *97-8*, 498.
[10] C. Delmas, M. Maccario, L. Croguennec, F. Le Cras, F. Weill, *Nature Mater.* **2008**, *7*, 665.
[11] L. Laffont, C. Delacourt, P. Gibot, M. Y. Wu, P. Kooyman, C. Masquelier, J. M. Tarascon, *Chem. Mater.* **2006**, *18*, 5520.
[12] G. K. Singh, G. Ceder, M. Z. Bazant, *Electrochim. Acta* **2008**, *53*, 7599.
[13] Y. M. Chiang, *Science* **2010**, *330*, 1485.
[14] R. Malik, F. Zhou, G. Ceder, *Nature Mater.* **2011**, *10*, 587.
[15] P. Bai, D. A. Cogswell, M. Z. Bazant, *Nano Lett.* **2011**, *11*, 4890.
[16] P. Gibot, M. Casas-Cabanas, L. Laffont, S. Levasseur, P. Carlach, S. Hamelet, J.-M. Tarascon, C. Masquelier, *Nature Mater.* **2008**, *7*, 741.
[17] M. Tang, W. C. Carter, J. F. Belak, Y. M. Chiang, *Electrochim. Acta* **2010**, *56*, 969.
[18] W. Dreyer, J. Jamnik, C. Guhlke, R. Huth, J. Moskon, M. Gaberscek, *Nature Mater.* **2010**, *9*, 448.
[19] L. Gu, C. Zhu, H. Li, Y. Yu, C. Li, S. Tsukimoto, J. Maier, Y. Ikuhara, *J. Am. Chem. Soc.* **2011**, *133*, 4661.
[20] D. Morgan, A. Van der Ven, A. G. Ceder, *Electrochem. Solid State Lett.* **2004**, *7*, A30.
[21] M. S. Islam, D. J. Driscoll, C. A. J. Fisher, P. R. Slater, *Chem. Mater.* **2005**, *17*, 5085.
[22] J. L. Allen, T. R. Jow, J. Wolfenstine, *Chem. Mater.* **2007**, *19*, 2108.
[23] G. Y. Chen, X. Y. Song, T. J. Richardson, *Electrochem. Solid State Lett.* **2006**, *9*, A295.
[24] X. H. Liu, H. Zheng, L. Zhong, S. Huang, K. Karki, L. Q. Zhang, Y. Liu, A. Kushima, W. T. Liang, J. W. Wang, J.-H. Cho, E. Epstein, S. A. Dayeh, S. T. Picraux, T. Zhu, J. Li, J. P. Sullivan, J. Cumings, C. Wang, S. X. Mao, Z. Z. Ye, S. Zhang, J. Y. Huang, *Nano Lett.* **2011**, *11*, 3312.
[25] X. H. Liu, Y. Liu, A. Kushima, S. Zhang, T. Zhu, J. Li, J. Y. Huang, *Adv. Energy Mater.* **2012**, *2*, 722.
[26] K. Dokko, S. Koizumi, H. Nakano, K. Kanamura, *J. Mater. Chem.* **2007**, *17*, 4803.
[27] K. Weichert, W. Sigle, P. A. Van Aken, J. Jamnik, C. Zhu, R. Amin, T. Acarturk, U. Starke, J. Maier, *J. Am. Chem. Soc.* **2012**, *134*, 2988.
[28] N. Meethong, H. Y. S. Huang, S. A. Speakman, W. C. Carter, Y. M. Chiang, *Adv. Funct. Mater.* **2007**, *17*, 1115.
[29] D. A. Cogswell, M. Z. Bazant, *ACS Nano* **2012**, *6*, 2215.
[30] R. Malik, D. Burch, M. Z. Bazant, G. Ceder, *Nano Lett.* **2010**, *10*, 4123.
[31] M. Z. Bazant, *Phase-field theory of ion intercalation kinetics*, arXiv:1208.1587v1.
[32] T. R. Ferguson, M. Z. Bazant, *J. Electrochem. Soc.* **2012**, *159*, A1967.
[33] T. Zhu, J. Li, *Prog. Mater. Sci.* **2010**, *55*, 710.
[34] J. Y. Huang, L. Zhong, C. M. Wang, J. P. Sullivan, W. Xu, L. Q. Zhang, S. X. Mao, N. S. Hudak, X. H. Liu, A. Subramanian, H. Fan, L. Qi, A. Kushima, J. Li, *Science* **2010**, *330*, 1515.
[35] S. W. Nam, H. S. Chung, L. C. Yu, Q. Liang, J. Li, Y. Lu, A. T. C. Johnson, Y. Jung, P. Nukala, R. Agarwal, *Science* **2012**, *336*, 1561.

ADVANCED MATERIALS

Supporting Information

for *Adv. Mater.*, DOI: 10.1002/adma.201301374

In Situ Atomic-Scale Imaging of Phase Boundary Migration in FePO 4 Microparticles during Electrochemical Lithiation

*Yujie Zhu , Jiang Wei Wang , Yang Liu , Xiaohua Liu , Akihiro Kushima , Yihang Liu , Yunhua Xu , Scott X. Mao , Ju Li , * Chunsheng Wang , * and Jian Yu Huang **

Submitted to ADVANCED MATERIALS

Supporting Information

In situ atomic-scale imaging of phase boundary migration in $FePO_4$ microparticles during electrochemical lithiation

Yujie Zhu, Jiang Wei Wang, Yang Liu, Xiaohua Liu, Akihiro Kushima, Yihang, Liu, Yunhua, Xu, Scott X. Mao, Ju Li, Chunsheng Wang,* and Jian Yu Huang**

Figure S1 shows the X-ray diffraction (XRD) patterns for $LiFePO_4$ and $FePO_4$. The XRD patterns were recorded by Bruker Smart1000 (Bruker AXS Inc., USA) using CuKα radiation source operated at 40 kV and 40 mA.

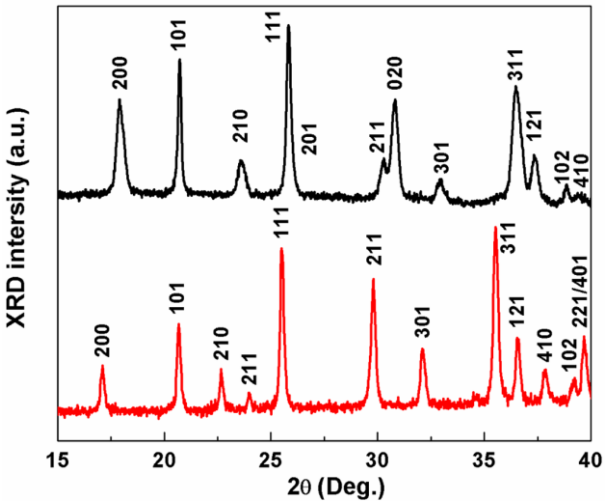

Figure S1. XRD patterns for synthesized $LiFePO_4$ and chemically delithiated $FePO_4$. The red and black lines are corresponding to $LiFePO_4$ and $FePO_4$, respectively. Both XRD patterns were indexed in the orthorhombic (*Pnma*) crystallographic system and showed that there were no detectable impurities in the samples.

Figure S2 shows the SEM images for the $FePO_4$ sample, which were taken by Hitachi SU-70 analytical ultra-high resolution SEM (Japan).

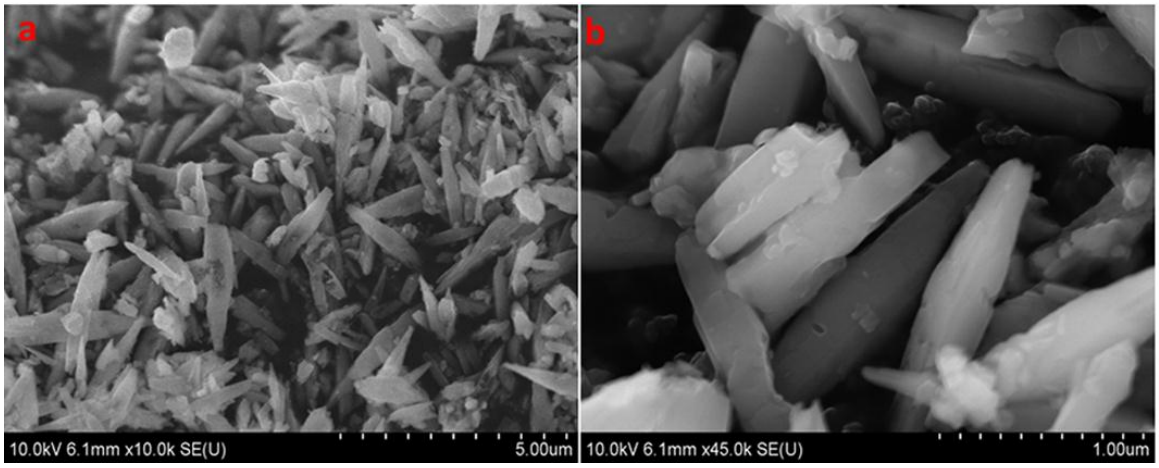

Figure S2. SEM images for $FePO_4$ sample. (a,b) SEM images of pristine $FePO_4$ sample.

Galvanostatic charge/discharge tests for $FePO_4$ electrodes

The hydrothermally synthesized $LiFePO_4$ was coated with carbon by ball milling the as-prepared $LiFePO_4$ with 20 wt. % sucrose in acetone for 1 h. The mixture was then heated to 600 °C for 5 h under Ar atmosphere with a heating rate of 2 °C/min. The $FePO_4$ sample was prepared by chemically delithiating above carbon-coated $LiFePO_4$ with nitronium tetrafluoroborate (NO_2BF_4) in acetonitrile.

$FePO_4$ electrodes were prepared by the slurry coating method. The active material was mixed with 15 wt% carbon black and 8 wt% polyvinylidene fluoride (PVDF) in 1-methyl-2-pyrrolidinone (NMP) solvent to form a viscous paste, which was then mixed for 30 min using a planetary ball milling machine. The obtained slurry was then coated onto aluminum foil and dried in a vacuum oven at 100 °C for overnight. The loading amount of the active material was 1-2 mg/cm^2. A coin cell consisting of a $FePO_4$ cathode, a Li metal anode, Celgard 3501 microporous film separators, and 1.0 M $LiPF_6$ in ethylene carbonate (EC): diethyl carbonate (DEC) (1:1 by volume) liquid electrolyte was used for electrochemical measurement. The galvanostatic charge/discharge tests with different specific currents were performed by using Solatron 1260/1287 Electrochemical Interface (Solatron Metrology, UK), and the results were shown in **Figure S3**.

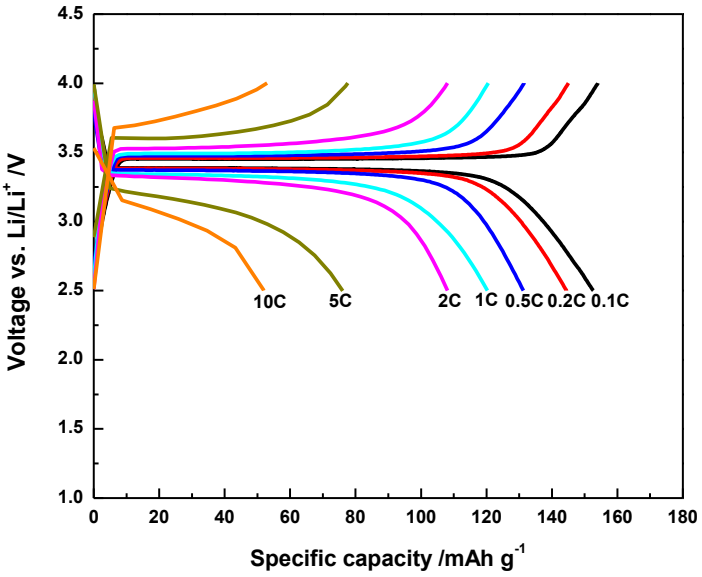

Figure S3. Galvanostatic charge-discharge curves for $FePO_4$ sample at different currents. Note: different C-rates are calculated one the basis of the theoretical capacity of $LiFePO_4$ (170 mAh g^{-1}).

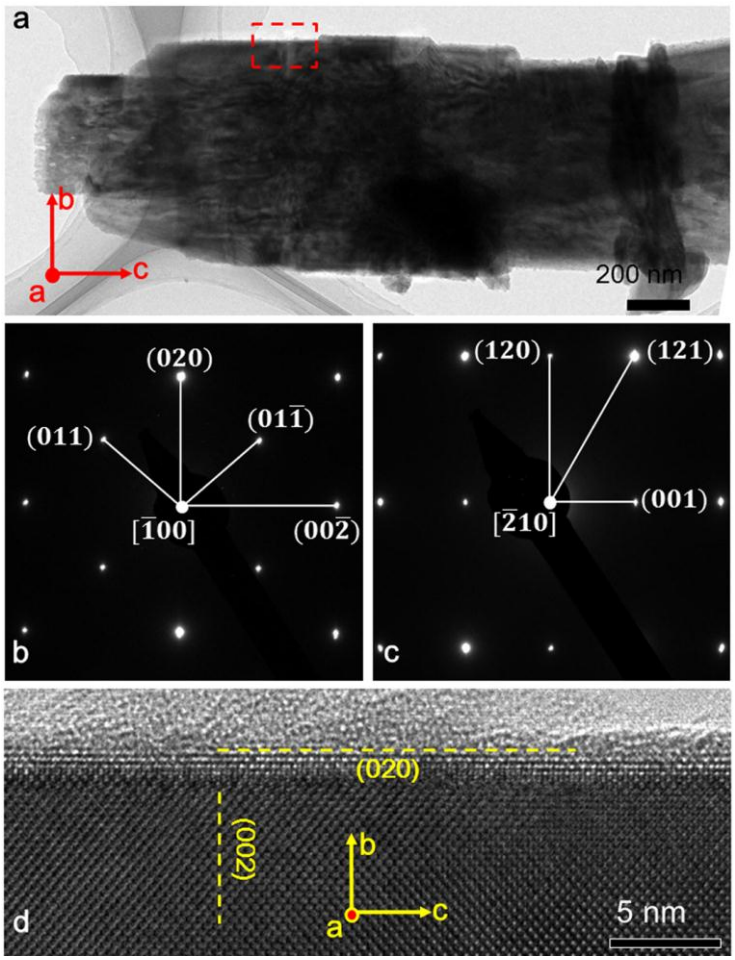

Figure S4. Determination of crystal orientation for the $FePO_4$ crystals. (a) Morphology of a typical $FePO_4$ crystal with *a*, *b* and *c* directions. (b,c) Two zone axes of the $FePO_4$ crystal in (a) were achieved by using double tilt holder. The EDPs are indexed with the lattice parameters: a = 9.826 Å, b=5.794 Å, and c=4.784 Å, and can be indexed as $[\bar{1}00]$ zone axis for (b) and $[\bar{2}10]$ zone axis for (c) with the orthorhombic structure, respectively. The EDPs indicate that the $FePO_4$ crystal is single-crystal with the *c*-axis parallel to the length direction. (d) HRTEM image from the red dashed line rectangle zone in (a), which is tilted into $[\bar{1}00]$ zone axis. (020) plane and (002) plane are parallel and perpendicular to the length direction of the $FePO_4$ crystal, respectively, which confirms that the *c*-axis is along the length direction of present samples.

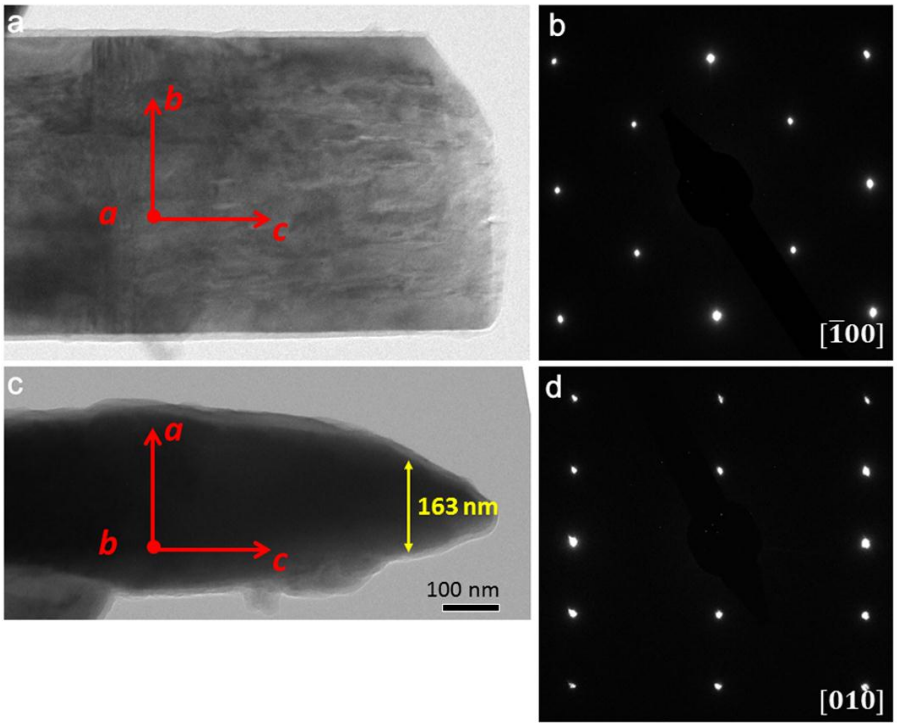

Figure S5. A typical $FePO_4$ particle tilted into both [$\bar{1}$00] and [010] zone axes. (a,b) The morphology and diffraction pattern of $FePO_4$ particle in [$\bar{1}$00] zone axis. (c,d) The morphology and diffraction pattern of $FePO_4$ particle in [010] zone axis with the thickness along a-axis (~160 nm) for the region, where $FePO_4$/$LiFePO_4$ phase boundary was observed, is marked.

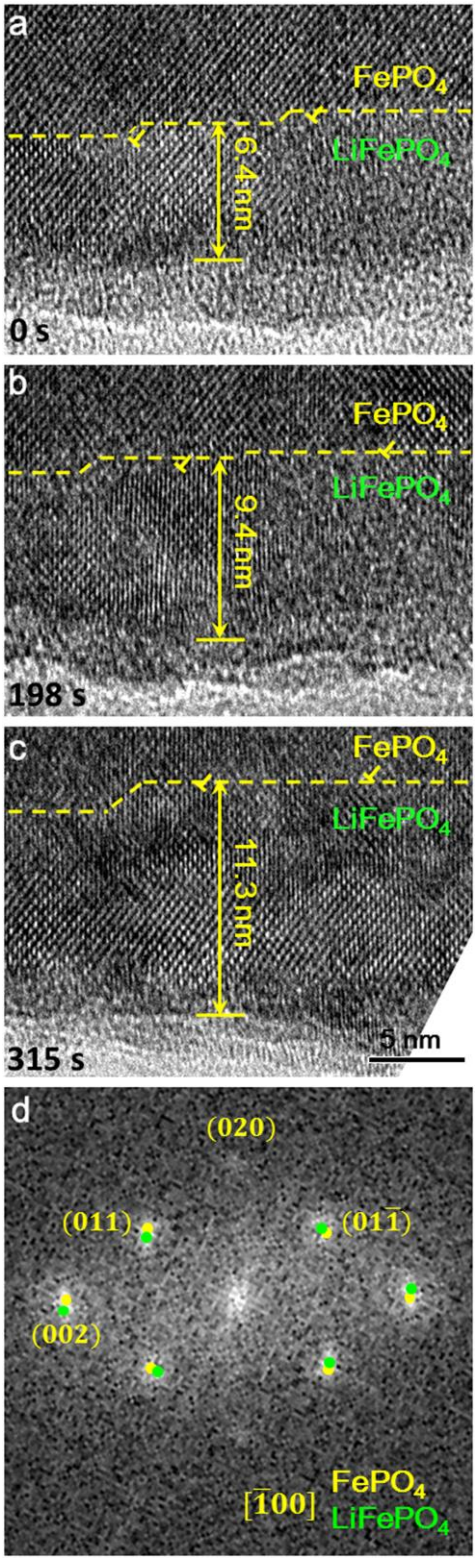

Figure S6. The sequential images showing the thickness of $LiFePO_4$ increased from 6.4 nm to 11.3 nm during further *in situ* lithiation of $FePO_4$ particle presented in Figure 2. (a-c) Some dislocations are observed at the $LiFePO_4/FePO_4$ phase boundary. (d) The FFT pattern obtained from $LiFePO_4/FePO_4$ zone shows two sets of FFT patterns.

Estimation of discharge C-rate for the particle in Figure 2

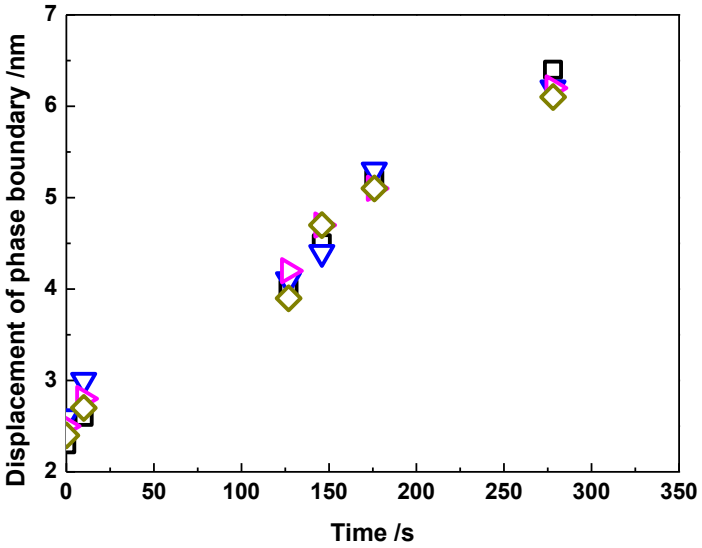

Figure S7. Displacement of phase boundary versus time during dynamic lithiation for $FePO_4$ single-crystal presented in Figure 2. Different symbols represent different segments on the phase boundary.

From **Figure S7**, here we show estimation of the corresponding C-rate for the particle presented in Fig. 2 by using the following equations:

$$I_{ave} \cdot \rho \cdot V_p \cdot t = Q_{th} \cdot \rho \cdot V_{LFP} \qquad \text{(Equation S1)}$$

with $V_p = a \cdot b \cdot c$ and $V_{LFP} = a \cdot c \cdot L$, where V_p and V_{LFP} are the volumes of pristine $FePO_4$ and $LiFePO_4$ transformed from $FePO_4$, respectively, L is the displacement of the phase boundary (4.3 nm), t is the time of observation (275 s=0.0764 h), ρ is the density of $LiFePO_4$ (3.6 g cm^{-3}), a, b, and c are the length of the particle along a-axis (300 nm), b-axis (600 nm) and c-axis (2860 nm), respectively, Q_{th} is the theoretical specific capacity for $LiFePO_4$ (170 mAh g^{-1}), and I_{ave} is the average discharge current for the particle (mA g^{-1}).

Inserting the above data into equation (Eq. S1), we get: $I_{ave} = \frac{170 \times 4.3}{600 \times 0.0764} \approx 16$ (mA g^{-1}).

The average discharge current corresponds roughly to 0.1C discharge rate.

Electron energy loss spectroscopy (EELS) for the particle in Figure 2

Figure S8 shows the EELS results for the Fe-$L_{2,3}$ (Figure S8a) and the O-K (Figure S8b) edge spectra of the pristine $FePO_4$ and the $LiFePO_4$ generated by *in situ* lithiation in Figure S6c. For the Fe-$L_{2,3}$ spectra (Figure S8a), strong L_3 and L_2 lines were observed and the maxima of L_3 and L_2 lines were separted by about 12 eV, which is consistent with literature.[1] Peak shifts about 1.8 eV have also been observed at the maximum of the Fe-L_3 line between $FePO_4$ and $LiFePO_4$ which is a charateristic behavior of changed Fe valence state.[1] The O-K edge (Figure S8b) for pristine $FePO_4$ shows a clear initial peak (marked as A in Figure S8b), whereas $LiFePO_4$ with Fe^{2+} is lack of this feature. Our O-K edge spectra for $FePO_4$ and $LiFePO_4$ are consistent with the results reported in literature. According to Laffont *et al.*,[1] this A peak indicates the valence state of iron in $LiFePO_4/FePO_4$ system. Both Fe-$L_{2,3}$ and O-K edge spectra confirm that the lithiated phase is $LiFePO_4$ and the observed phase boundary is the $LiFePO_4/FePO_4$ phase boundary.

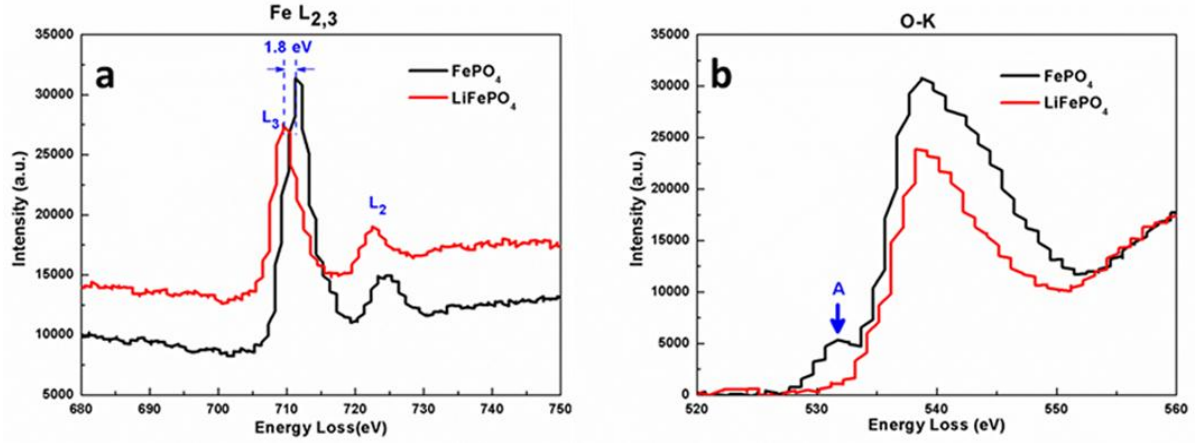

Figure S8. EELS results for the particle shown in Figure 2. (a,b) Fe-$L_{2,3}$ and O-K edge spectra of pristine $FePO_4$ and $LiFePO_4$ generated by *in situ* lithiation.

Data processing procedure for HRTEM images

To make sure what we observed was truly phase boundary rather than some artifacts, we used four measures for confirmation, which are established and also widely used for analysis of HRTEM images about phase boundaries in different materials.

(1) **Contrast difference**. Such contrast difference is usually associated with some changes in the material, such as composition, thickness, orientation with respect to the incident electron beam, or their combinations. Compositional changes can be perceived from very large to very small length scales. At small length scales, as in HRTEM images of a system containing several phases, the contrast is different across the phase boundaries due to the different crystal fields that modulate propagation of the incident electron beam, even on a width of 1 nm such as an atomically sharp interface. When the Li ions insert into an anode material, such as Si,[2] a sharp phase boundary is produced and the lithiated part has the brighter contrast. Similar to the case of Li diffusion into $FePO_4$, in the *in situ* heating of Si nanodevices, a sharp phase boundary is created when Ni atoms diffused from the Ni contact-side into the Si nanowires by forming $NiSi_2$ phase.[3] For $LiFePO_4/FePO_4$ system, same contrast difference across the phase boundary has been observed in the *ex situ* experiments,[1,4,5] *i.e.* in which the $LiFePO_4$ region showed a lighter contrast than the $FePO_4$. The contrast difference induced by the atomic weight (i.e., different atomic scattering factors) is also observed in other materials, such as AlAs-GaAs and Al-Pb.[6,7] The contrast difference tells us the location where a phase boundary may exist.

(2) **Lattice spacing difference between different phases.** The $LiFePO_4/FePO_4$ phase boundary is such a kind of interface that the two phases have almost the same orientation on two sides.[3-5] However, the spacing difference, despite small, is measurable. The measured lattice spacings are shown in Figures 2e-f and 3g-h. This method is also frequently used in the analysis of $LiFePO_4/FePO_4$ two-phase systems.[4,5]

(3) **Fast Fourier Transform (FFT) analysis.** Power spectrum (i.e. FFT pattern) is generated from the HRTEM, which directly visualizes tiny difference of atomic arrangements of the closely related phases. Two sets of diffraction patterns were observed and indexed to $LiFePO_4$ and $FePO_4$, respectively, which confirms that the interface we observed was truly a $LiFePO_4/FePO_4$ phase boundary. Figure 2d is the FFT image computer-generated by using the Gatan DigitalMicrograph® software, which was the general method used to analyze the HRTEM images of $LiFePO_4$ and $FePO_4$.[1,4,5]

(4) **Misfit dislocations.** The mismatch between $LiFePO_4$ and $FePO_4$ might produce misfit dislocations at the phase boundary, which are shown as the extra half atom planes. Such misfit dislocations are the most important feature for most phase boundaries, such as Al-Pb, $SrZrO_3$-$SrTiO_3$ and GaSb-GaAs.[7-9] For the $LiFePO_4/FePO_4$ system, the well-organized extra half planes show up at the $FePO_4$ side due to the smaller lattice spacing, as shown in Figure 2c and Figure 3d, and such dislocations are distributed at expected densities in agreement with the amount of lattice mismatch of the given interfaces. This corroborates that the interface we observed undoubtedly is the $LiFePO_4/FePO_4$ phase boundary.

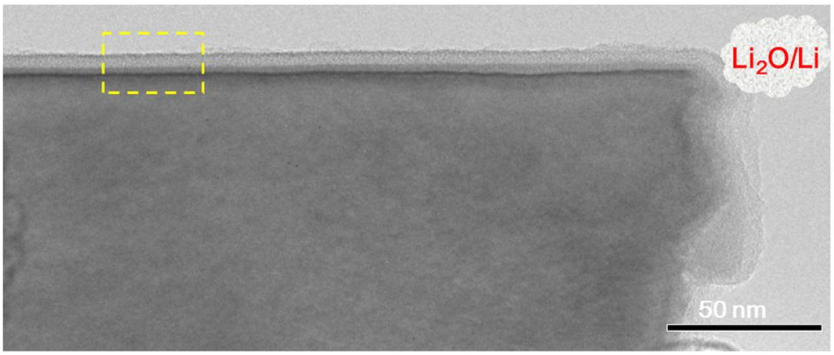

Figure S9. Pristine $FePO_4$ particle used in Figure 3. The pristine carbon-coated $FePO_4$ sub-micron particle with no crack and uniform thickness, as demonstrated by the uniform contrast. The yellow dashed line marked the region, where the HRTEM images in Figure 3, were taken.

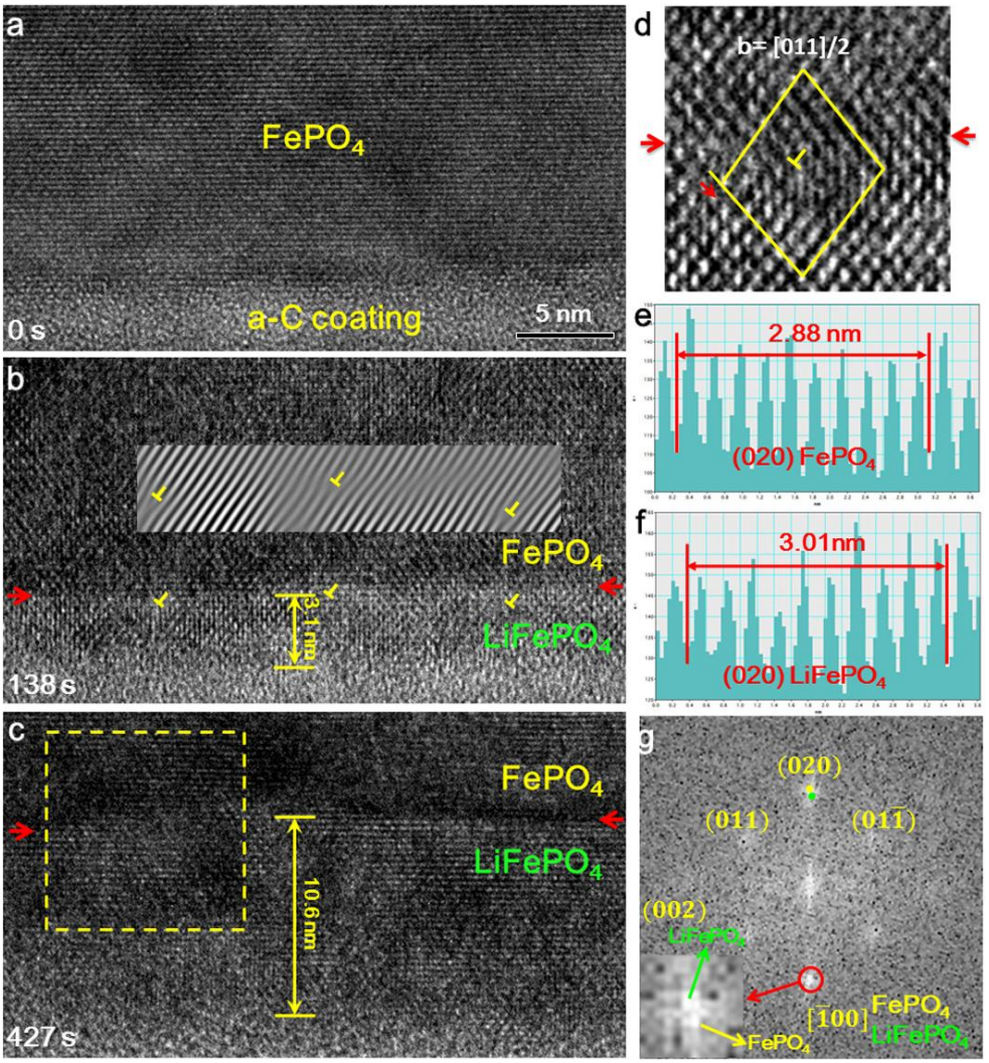

Figure S10. Migration of phase boundary between $FePO_4$ and $LiFePO_4$ along the [010] direction during lithiation. (a) The pristine $FePO_4$ with a-C coating. (b) At 138 s, 3.1 nm $LiFePO_4$ was developed due to lithiation. A clear phase boundary between $FePO_4$ and $LiFePO_4$ was formed, as pointed out by the red arrows. The misfit dislocations were uniformly distributed near the phase boundary between $FePO_4$ and $LiFePO_4$, as marked out by the reversed "T". The insert is the IFFT showing the dislocations at the phase boundary. (c) At 427 s, the thickness of $LiFePO_4$ layer increased to 10.6 nm. The phase boundary moved along [010] direction, which is perpendicular to the [020] plane. (d) The Burger's vector of mismatch dislocation are identified to be [011]/2. (e,f) Lattice spacing of (020) plane for $FePO_4$ and $LiFePO_4$ respectively, which was measured from HRTEM image shown in (c). The lattice spacing of (020) plane increased about 4.2% after lithium ion insertion into $FePO_4$. (g) The FFT patterns produced from $FePO_4$ and $LiFePO_4$ regions marked by yellow dashed line in (c). Clearly, the spots of (020) plane split into two spots at each diffraction point. Note: a positive voltage of 2.5 V versus lithium metal was applied to the $FePO_4$ crystal.

References

1. L. Laffont, C. Delacourt, P. Gibot, M. Y. Wu, P. Kooyman, C. Masquelier, J. M. Tarascon, *Chem. Mater.* **2006**, *18*, 5520.

2. X. H. Liu, J. Y. Huang, *Energy Environ. Sci.* **2011**, *4*, 3844.

3. W. Tang, S. A. Dayeh, S. T. Picraux, J. Y. Huang, K-N. Tu, *Nano Lett.* **2012**, *12*, 3979.

4. C. V. Ramana, A. Mauger, F. Gendron, C. M. Julien, K. Zaghib, *J. Power Sources* **2009**, *187*, 555.

5. G. Y. Chen, X. Y. Song, T. J. Richardson, *Electrochem. Solid State Lett.* **2006**, *9*, A295.

6. W. Braun, A. Trampert, L. Daweritz, K. H. Ploog, *Phys. Rev. B.* **1997**, *55*, 1689.

7. H. Rosner, J. Weissmuller, G. Wilde, *Philosophical Magazine Letters.* **2006**, *86*, 623.

8. F. Ernst, A. Recnik, P. A. Langjahr, P. D. Nellist, M. Ruhle, *Acta Mater.* **1999**, *47*, 183.

9. Y. Wang, P. Ruterana, L. Desplanque, S. E. Kazzi, X. Wallart, *EPL*, **2012**, *97*, 98011P1.